Microstructures of titanium oxide thin films grown continuously on stainless steel wires by PVD in an inverted cylindrical magnetron: Towards an industrial process

C. Esparza-Contro, G. Berthomé, G. Renou, F. Robaut, S. Coindeau, C. Vachey, J. Cambin, M. Mantel, L. Latu-Romain

Version of Record: https://www.sciencedirect.com/science/article/pii/S0257897220303121
Manuscript_3fa194b332dafebb88e3cff8e70c3a57

Microstructures of titanium oxide thin films grown continuously on stainless steel wires by PVD in an inverted cylindrical magnetron: towards an industrial process

C. Esparza-Contro[1,2], G. Berthomé[1], G. Renou[1], F. Robaut[1], S. Coindeau[1], C. Vachey[2], J. Cambin[2], M. Mantel[1,2], L. Latu Romain[1,2]

[1] Univ. Grenoble Alpes, CNRS, Grenoble INP, SIMaP, F-38000 Grenoble, France

[2] Ugitech S.A., Avenue Paul Girod, 73403 Ugine Cedex, France

Abstract

Producing colored coatings by Physical Vapor Deposition (PVD) in an in-line way is an interesting industrializing process. Moreover, the durability of vacuum coatings is an advantage for architectural applications such as outdoor decoration. In this project, titanium dioxide coatings were produced over moving stainless steel wires via direct current (DC) reactive magnetron sputtering PVD in an inverted cylindrical magnetron. The samples were characterized by transmission electron microscopy (TEM) coupled with ASTAR (Automated crystal orientation mapping on TEM -ACOM- with precession tool -DigiSTAR-) orientation-phase mapping and EDS (Energy Dispersive X-Ray Spectroscopy) chemical mapping. The microstructure of TiO_x thin films is analyzed as a function of the O_2 flux in the chamber. In the metallic mode, a 300 nm polycrystalline hexagonal Ti film is obtained in 2 min 30 s at 1000 W. For the same power and same time but in the poisoned mode, a 40 nm titanium dioxide film composed of both rutile and anatase columnar grains is obtained. A peculiar mode is the transition one, where in a single pass through the chamber a multilayer of ≈ 230 nm hexagonal Ti and ≈ 70 nm pure rutile titanium dioxide is grown. This multilayer is a result of a heterogeneous magnetic field, hence of the chamber poisoning. All these thin films present chemical, structure and grain size gradients because of an original process (in-line and cylindrical inverted magnetron) with plasma density heterogeneity.

Keywords: Titanium dioxide, reactive magnetron sputtering, Physical Vapor Deposition, TEM-ASTAR orientation and phase maps, inverted cylindrical magnetron, stainless steel

1. Introduction

Modern architecture can be interested by the decoration of some walls with colored stainless steel wires weaving made in thin films over these metallic structures. These thin films may have various chemistries as TiN [1], ZrN [2], a mixture of both TiN/ZrN [3], TiO_xN_y [4], FeN_xO_y [5]. These materials can be grown by various techniques such as sol-gel [6], chemical vapor deposition (CVD) [7], and physical vapor deposition (PVD) [8].

This study will focus on titanium oxides TiO_x grown by Physical Vapor Deposition (PVD). The choice of titanium dioxide as thin film is due to its various interesting surface properties. For instance, the color generation of titanium dioxide is the result of optical constructive interferences [9]. A part of the light is reflected at the external surface of the titanium dioxide coating whereas the other is reflected at the coating/substrate interface. The constructive interferences of the waves give a color depending only on the thickness of the coating. This physical property is interesting for industrial production, because for a same nature of compound, it is possible to have different colors just by varying the thickness of the coating. Nevertheless, and for this industrial production, special attention has obviously to be paid to avoid modification of the color with the diminution of the thickness of the coating. Another interesting property of titanium dioxide is its semiconductor nature [10]. Titanium dioxide has a band-gap of 3.2 eV (for the anatase phase, and 2.95 eV for rutile), and has photocatalytic properties with UVs, which have a self-cleaning effect for the pieces that are exposed to sunlight. These properties are attractive for the market of decorative wires in architecture, which is one of the applications searched in this research project (Fig. 1).

In the present work, thin films are produced by PVD in an Inverted Cylindrical Magnetron (ICM), in order to coat homogeneously the surface of the wire, and continuously to respond to a logical process of coating a steel reel. In this project, titanium dioxide is made by reactive magnetron sputtering with a titanium target and oxygen as a reactive gas. When oxygen is

introduced with argon into the deposition chamber, two deposition modes can take place [11]. If the flux of oxygen is inferior to a critical value ϕ_c, it is consumed and does not saturate the target. In this case, the target remains metallic and the sputtering rate is not significantly changed. On the other hand, when the amount of oxygen increases ($>\phi_c$), the oxidation rate of the target is higher than its sputtering rate corresponding to an oxidized cathode. This is called the poisoned mode, and one of its characteristics is a lower deposition rate than in the metallic mode.

In the last decades, titanium dioxide thin films produced by PVD were proved to have a greater mechanical durability than by sol-gel method [12]. Since then, efforts have been done to determine the microstructures of titanium dioxide coatings in link with the deposition parameters process [13]. The first step is to produce stoichiometric titanium dioxide, which is achieved without control issues when working in poisoned mode. Nevertheless, to produce it at high deposition rates it can be wished to coat in the transition mode [14] (corresponding to the regime between the metallic and the poisoned modes), even though this mode is unstable. To attain stability in this capricious mode, control process has been developed, and even industrialized [15]. Once titanium dioxide is obtained it is necessary to have the adequate microstructure; for instance, rutile for optical applications due to its high refractive index [16]. Let's remind that it is hard to refer to thermodynamics in PVD conditions but it is still useful. The stable phase of titanium dioxide is rutile [17,18] whereas anatase and brookite are metastable phases. When anatase is created its transition to rutile varies from 400 to 1000 °C as a function of the oxidizing atmosphere and the impurities present in the titanium dioxide [19]. To achieve and control crystallization in PVD, the necessary energy input may be provided by the bombardment of energetic particles or by heating the substrate [11]. Precise measurements have been done in the literature where an energy of about 7 keV per deposited atom was needed to grow an anatase structure [20]. More energy leads to a rutile/anatase

mixture with increasing relative quantity of rutile, but less would result in an amorphous coating [20]. In an in-line process, it is also possible to obtain crystallization with post-annealing or by coating with a reactive medium frequency pulse magnetron in order to avoid a substrate heating at more than 300 °C [21] (the different kinds of current pulses of this experiment are described in detail in [22]). In this project, crystallized TiO_x thin films are produced in-line without post-annealing nor medium frequency current pulses, but with a substrate temperature > 300 °C, inherent to the process and not to external heating.

The magnetron technology facilitates the conservation of a plasma discharge at a low pressure, but it localizes it in space, too. The magnetron used in this project provokes a heterogeneous magnetic field, so a heterogeneous deposition rate. For an in-line process, where the substrate traverses the chamber, the final coating is the sum of these deposition rates done in a continuous process, which permits to obtain a multilayer coating in a reel with a homogeneous thickness. The objective of this paper is to draw the various compositions and microstructures, partly described by TEM-ASTAR [23], as a function of oxygen partial pressure obtained by the original process described above. The final goal is to obtain interferometric thin films on stainless steel wires, towards an industrial process, to attain a colored wire.

2. Material and methods

2.1 Coating deposition – PVD process

The coatings were deposited on moving 316L stainless steel wire substrates with a diameter of 2.09 mm. These substrates have an industrial finish (mean rugosity of 1 µm) and a composition given in Table I.

The wire moved at a pace of 2 mm/s and passed one minute through a microwave plasma cleaning in 10% hydrogen diluted in argon atmosphere at 0.5 Pa (the used microwave plasma cleaning is described in detail in [24]) before entering the DC reactive magnetron sputtering

PVD chamber. The wire (substrate) was incorporated in a drawing line, so it was grounded for safety reasons.

A schematic view of the ICM chamber is shown in Fig. 2, and the process has already been described elsewhere [25,26]. In a few words, the moving stainless steel wire passed through a 30 cm water-cooled titanium target, corresponding to 150 s of deposition time. This target was surrounded by magnets (made in NdFeB in a balanced magnetron configuration), and the target-substrate distance was of 19 mm. It was necessary to add auxiliary anodes to collect the electrons that would instead be captured by the wire and would heat it [25]. If the anodes were polarized, the temperature of the substrate kept inferior to 350 °C. This temperature was measured via a pyrometer that was placed 280 mm after the deposition chamber. The values were corrected considering heat losses due to thermic radiation [25].

A DC power supply (Pinnacle Plus+ from Advanced Energy) was used in the current regulation mode with a cathodic current I_k of 2.75 A, which corresponded to 7.3 mA/cm^2, unless specified. The corresponding cathodic voltage V_k and power P were given when samples were introduced. For the anodes, a DC power supply (Chroma) was used in a voltage regulation mode with a voltage V_A of 30 V, unless specified.

The samples described in Table II were obtained by varying the oxygen flow ϕ_{O_2} in the chamber, while the argon flow ϕ_{Ar} was kept constant at 16.5 sccm. The pressure of Ar p(Ar) was fixed at 0.67 Pa with the opening of the vacuum valves. Gases were introduced at the center of the chamber whereas the pumping system was at each extremity of the chamber. Almost all the characterizations were done in the continuous process described above. The exception was for the static coatings, which were produced with the same discharge conditions, but over an immobile substrate.

2.2 Characterizations

In this work, the presented structural and chemical characterizations are mainly coming from Transmission Electron Microscope (TEM) observations of thin lamella (priory prepared by FIB-SEM -Focused Ion Beam-). Nevertheless, former work on the samples was necessary to identify the present phases with its respective chemical composition: thin films have been first characterized by complementary physico-chemical techniques as Grazing Incidence X-Ray Diffraction (GIXRD), Raman Spectroscopy, Energy Dispersive X-Ray Spectroscopy (EDS), and Scanning Electron Microscope (SEM) observations.

X-Ray diffraction was done in grazing incidence at 1.2° using a PANalytical X'Pert PRO MPD diffractometer from CuKα wavelengths. The identified phases (space group, lattice constant) are α-Ti (P63/mmc, a = 2.949 Å, c = 4.695 Å), α-$TiO_{x<0.2}$ (P63/mmc, a = 2.970 Å, c = 4.753 Å), α-$TiO_{x<0.5}$ (P63/mmc, a = 2.973 Å, c = 4.839 Å), lava phase Ti_2(Fe,Ni) (Fd-3m, a = 11.338 Å), R-TiO_2 (rutile P42/mnm, a = 4.597 Å, c = 2.965 Å), A-TiO_2 (anatase I41/amd, a = 3.807 Å, c = 9.090 Å), and the austenitic stainless steel (Fm-3m, a = 3.497 Å). GIXRD results of coatings produced at different modes – pure titanium, metallic, transition, and poisoned – are displayed in the Fig. 3. The crystallographic data are needed to provide proper information to the database in order to achieve the TEM-ASTAR (Automated crystal orientation mapping on TEM –ACOM- with precession tool –DigiSTAR-) analysis, which will permit to draw orientation and phase maps with a nanometric resolution.

To distinguish clearly the two titanium dioxide structures, anatase and rutile, Raman spectroscopy was punctually used in a Renishaw spectrometer with an Argon laser (λ = 514.5 nm) in a surface of approximately 1 μm^2, traversing the whole thickness of the coating.

The EDS measurements achieved in the SEM allowed also to determine the thickness of the pure titanium coating. EDS spectra (of a sample area of 425 µm x 570 µm) are taken at various energies on the coated wire (from 10 to 20 keV); and as a function of Ti/Fe intensity ratio, coupled with Stratagem software [25], the thickness of the coating can be determined.

Of course the density and the nature of the coating and substrate need to be known. This 'indirect' method has been compared with the 'direct' one (consisted by the preparation of transversal cross-section followed by direct thickness measurement in the SEM). This method is totally satisfactory for the titanium/stainless steel system.

The mapping technique in the TEM, ASTAR [23], was used to determine the crystallographic orientation and the phases, here on transversal cross-section. To produce the 50 nm thick lamella, the system coating/substrate was machined in a dual focused ion beam scanning electron microscope. After, in the TEM, a selected zone was scanned: the diffraction pattern was recorded with a 1 nm probe size and a 3 nm step size. Finally, each pattern was compared to a database in order to fit with the appropriate crystalline structure and orientation.

3. Results and discussion

First, in order to understand the consequence of the in-line process on the final constitution of the thin film, a titanium coating grown while the stainless steel wire stands still (static mode) or while the substrate is moving (dynamic mode) is described. Then, titanium oxides coatings grown at different oxygen flows will be described in the dynamic mode (in-line process).

3.1 Microstucture vs. hysteresis of $p(O_2)$

3.1.1 Static vs. dynamic

A static coating is produced when the wire is not moving, while a dynamic coating is produced when the wire passes through the cathode at a speed of 2 mm/s. The static coating gives the information of the deposition rate at each point. In this ICM, a static coating consists of 30 cm (size of the chamber) of stainless steel wire coated heterogeneously. The deposition rate is measured with a step of 1 cm by EDS in the SEM.

To compare a static coating vs. a dynamic coating, a pure titanium coating over the stainless steel substrate is used as an example. First, the morphology of the coating grown in a dynamic mode (Fig. 4) is described and its peculiar constitution is hereafter explained as a function of

the evolution of the deposition rate along the wire when this one stands still, the static mode (Fig. 5).

The SEM micrograph of a dynamic titanium coating at 0 sccm of oxygen flux observed in cross-section preliminary prepared by FIB is presented in the Fig. 4. The C protective layer (priory deposited in the FIB-SEM) is seen at the top while the stainless steel substrate is at the bottom of the image. In between, a Ti coating is revealed with three sub-films.

These sub-films may be explained by analyzing the way in which the dynamic coating was grown by comparing it with a static coating. To understand the architecture, the deposition rate along the 30 cm length of the wire grown in a static mode is given in Fig. 5 for a pure titanium coating.

There are two maxima of the deposition rate as a function of the axial position in the chamber. In fact, this coating is deposed essentially in two times: at the beginning and at the end of the cathode. These zones of high deposition rate can be recognized in the cross-section observation (Fig. 4). The heterogeneity of the deposition rate is due to the heterogeneity of the magnetic field (Fig. 6).

The plasma, the sputtering rate, and the deposition rate are more intense in the extremities due to the presence of the anodes, which collect the electrons. Therefore, there are less electrons in the center of the chamber, that is to say a lower density plasma and as a consequence a lower sputtering rate at this place. In the case of titanium, which reacts readily with oxygen, the areas of the center where the plasma is less intense will poison with the oxygen present in the leaks inherent to the continuous process. Therefore, the center of the cathode has a non-zero deposition rate of compound. This is the zone of low deposition rate in Fig. 4, which is darker than the Ti zones because of its oxygen content. It is well-known that in the poisoned mode, the deposition rate is lower than in the metallic mode [27]. The effect of plasma

heterogeneity is demonstrated by the racetracks of preferential sputtering observed in the cathode after 10 hours of service (Fig. 7).

The objective of a static experiment is to figure out the heterogeneities in the chamber when the coatings are produced. When these heterogeneities are constant with time, the dynamic coating formed when the wire is in movement is homogeneous along the wire length. Now the study will focus only on dynamic experiments where the wire is moving at 2 mm/s.

3.1.2 Dynamic as a function of hysteresis

The classic hysteresis experiment is achieved with a cathode power stabilized at 1000 W (Fig. 8). The experiment consists in increasing the oxygen flow each 2 minutes and a half, and record parameters such as the discharge voltage, until the poisoned mode is obtained. Finally, the oxygen flow is decreased by stages, too. The hysteresis experiment is repeated at a constant current of 3 A, and the same curve is obtained.

In this ICM chamber, the final color of the samples permits to determine that increasing the oxygen flow results in different coatings. From 0 to 1 sccm, a gray color is observed; from 1.1 to 2 sccm, a blue color; and beyond 2.15 sccm, coatings are brown (colors at the top of Fig. 8). For this experiment, the value of the power remained constant at 1000 W.

Each of the three colors corresponds to a value of discharge voltage (upper part of Fig. 8). The cathode voltage V_k increases as oxygen flux is increased. It corresponds to a normal behavior, because the chemisorption of oxygen on the surface of the cathode decreases the secondary electron emission yield γ [27], and $V_k \propto \gamma^{-1}$ [28]. However, there is an intermediate value of the discharge voltage between the metallic and poisoned modes. It corresponds in fact to a partial poisoning between 1.1 and 2 sccm of oxygen flux.

The chemical compositions, the structures and grain orientations of thin films grown in the metallic, transition, and poisoned modes are next described. It is important to already underline that whereas the coated wire has a homogeneous color, original gradients in term of

microstructure, phases and chemical composition are obtained, because of the in-line heterogeneous process.

3.1.2.1 Metallic mode

The Fig. 9 shows bright-field STEM images with EDS maps and TEM-ASTAR phase and orientation maps from a metallic coating grown at an oxygen flow of 0.5 sccm. This coating has a thickness of 260 nm, corresponding to a deposition rate of 1.8 nm/s and is composed of two titanium films separated by an interface of Ti richer in oxygen as shown in the EDS map (Fig. 9a) of 40 nm. This coating results of the partial poisoning of the cylindrical target: two metallic zones where Ti is sputtered in the extremities of the chamber and a poisoned zone at the center of the chamber.

This transition Ti film rich in oxygen is difficult to characterize because of very small grains (13 ± 3 nm), and for it is trapped between two metallic Ti films. Still, several information could be obtained from diverse characterization techniques. From ASTAR, the form of the diffraction pattern implies there is crystallization. Nevertheless, grains are too small for indexation to be reliable because the electron beam traverses more than 5 grains with different orientations. That is why the oxygen rich region corresponds to a darker zone on the ASTAR map coming from low index (in darker green in the phase map of Fig. 9). From GIXRD, only the Ti hexagonal phase, with the same lattice parameter as pure Ti, and the cubic 316L phases have been detected, therefore no TiO_x nor titanium dioxide can be observed with this technique. From Raman spectroscopy, no signal was obtained when the laser was focused on the top of the sample, nor on a cross-section, so no titanium dioxide is observed via this technique. We may conclude that the partial poisoning at the center yields a Ti coating with a titanium interlayer richer in oxygen in the middle of a sandwich, and for the moment titanium dioxide has not been observed in this final coating.

3.1.2.2 Transition mode

The Fig. 10 shows the STEM image and TEM-ASTAR maps of the transition mode done at an oxygen flux of 1.7 sccm. This coating is composed of a hexagonal $TiO_{0.2}$ film, Ti with interstitial oxygen deduced from GIXRD lattice parameters [29] [30] (Fig. 3), of 215 nm and a second film titanium dioxide rutile of 70 nm.

The titanium film was deposited in the first part of the cathode. Titanium grains are columnar (50-200 nm high with an aspect ratio of 0.3) with a slight preferential orientation along <0001> direction (red color on Fig. 10c). In fact, this first part of the cathode is the only part that remains metallic, the rest is poisoned, explaining the presence of a titanium dioxide film in the upper part. This upper part of the transition coating is indeed titanium dioxide film, which is deposited continuously after the titanium film in the same chamber. The titanium dioxide grains are smaller (5-30 nm) without preferential orientation.

Consequently, when the O_2 flux is increased to more than 1 sccm, one of the extremities of the cathode (in this case, the end) gets poisoned. For the transition mode, the coating is essentially deposed at the beginning of the chamber, where the mode is still metallic.

3.1.2.3 Poisoned mode

The poisoned coating of 40 nm is obtained at high oxygen partial pressure (oxygen flux > 2 sccm). The Fig. 11 shows a bright-field STEM image and TEM-ASTAR phase and orientation maps from a poisoned coating, which is composed of titanium dioxide of both anatase and rutile phases. It should be noted that the proportion of rutile grains is higher than the anatase one. The presence of anatase will be discussed in the next paragraph. Grains are columnar (10-40 nm high with an aspect ratio of 0.3). An interface 6-7 nm thick is visible between stainless steel and titanium dioxide. This interface is in fact the oxidation of the steel matrix in $(Fe,Cr)_2O_3$. A hypothesis to explain this formation of oxides is the diffusion of oxygen into the substrate at T > 350 °C or an oxidation of the substrate in the deposition chamber.

In poisoned mode, the whole cathode is covered by a stoichiometric titanium dioxide compound. In this case, the sputtering rate and deposition rate of titanium dioxide are decreased by a factor 9 compared to the deposition of Ti in metallic mode.

3.1.2.4 Sum-up

The Fig. 12, sumps-up the various heterostructures grown as a function of oxygen partial pressure.

At low oxygen flux, in the metallic mode, the stainless steel is coated firstly with a hexagonal Ti film, then of a rich in oxygen hexagonal Ti film (at the center of the cathode), and finally of a second hexagonal Ti film. When the oxygen partial pressure is increased to a transition mode, the high deposition rate zone of Ti at the end of the chamber gets poisoned. So, the stainless steel is covered by titanium as a first film when passing through the cathode, and by titanium dioxide in form of rutile as a second film. When the whole cathode is poisoned, a unique film of titanium dioxide of rutile and anatase is observed on the moving substrate.

For the transition mode, titanium dioxide do not only come from the sputtering of titanium dioxide in the poisoned zones of the cathode, but also by two other possible effects (non-excluding effects). The first phenomenon is the oxidation of titanium sublayer. This may be confirmed because when the temperature is modified, this titanium dioxide zone is thicker. The second phenomenon is the sputtering of Ti in a transition mode as described by Snyders corresponding to both condensation of sputtered Ti material and reaction between the growing film with the reactive oxygen species [27]. It explains why titanium dioxide is deposited at a higher deposition rate in the transition mode compare to the poisoned one (titanium dioxide film thickness is 70 nm -resp. 40 nm- in the transition -resp. poisoned- mode).

Various gradients of chemical composition and crystalline structures are obtained coming from the continuous growth mode associated to the heterogeneity of the plasma inside the cylindrical cathode.

3.2 Titanium interlayer effect on titanium dioxide grains nature

A test is done to verify the hypothesis that a Ti interlayer favors the rutile titanium dioxide phase (observed in the transition mode) in the conditions in which normally the titanium dioxide coating would crystallize in rutile and anatase (observed in the poisoned mode). This experience consists of adding a titanium layer between the titanium dioxide coating and the stainless steel (top of Fig. 13). For this, a first pass of pure titanium was made over the stainless steel. After, this wire repassed by the chamber, but in a poisoned mode condition (the same growing parameters as the poisoned mode already described). This new sample, 316L/titanium/poisoned titanium dioxide, and the already presented 316L/poisoned titanium dioxide are analyzed via Raman spectroscopy (Fig. 13). The wire with a titanium interlayer presents mainly rutile (Raman spectroscopy is very sensitive to anatase), while the wire without a titanium interlayer presents both anatase and rutile.

For higher energy fluxes or higher substrate temperatures, it is possible to have only rutile. If the energy is not too high, anatase is obtained. Indeed, anatase crystallizes faster than rutile, because it has a lower surface free energy [31]. For even less energy fluxes, an amorphous structure may be produced [32]. Löbl [32] explains that a higher elastic energy is necessary for the formation of a dense compound, indeed, $\rho_{amorphe}(3.2 - 3.65\ g\ cm^{-1}) < \rho_{anatase}(3.84\ g\ cm^{-1}) < \rho_{rutile}(4.26\ g\ cm^{-1})$.

With this test (Fig. 13), it is possible to conclude that a titanium interlayer favors the formation of rutile. This was already observed elsewhere [33], and the explanation that is given by Rama et al. is that the heterogeneous nucleation given by the titanium interlayer minimizes the surface energy and permits the rutile formation. Adding an interlayer of silver nanoparticles [34], SiO_2 [35], or others as a seeding layer induces nucleation sites, and it is well-known that a seed-layer can allow to control the microstructure [36]. The hypothesis of a

Ti interlayer permitting to grow a higher ratio of rutile/anatase is coherent with the transition mode, which consists of rutile over a hexagonal TiO_x film.

In this section, it was shown that titanium dioxide grains crystalline nature depends partly on the substrate; with hexagonal titanium substrate, rutile is grown preferentially than anatase (in the conditions where the titanium dioxide coating would crystallize in rutile and anatase).

3.3 Temperature effect

During a continuous PVD deposition where the wire is the anodic part of the system, it seems important to study the effects of the substrate temperature during the deposition. This wire temperature can be modified thanks to auxiliary anodes by keeping all other parameters similar. The modification of the plasma linked to the modifications in anode polarization is neglected in this part of the study.

If the substrate temperature is increased from 350 °C to more than 600 °C (when there is no polarization of the anodes), there is a modification of the substrate and of the coating during the deposition of the TiO_x films, described hereafter.

For the metallic and the transition modes, the same modifications to the substrate and to the Ti interface are observed when increasing the deposition temperature. STEM-EDS maps shown in Fig. 14 shows only the metallic mode. The increase temperature results in Fe and Ni diffusion from the stainless steel to the TiO_x thin film, and it leads to lava phases in the internal subscale (Fig. 14a). These lava phases were identified elsewhere [26] for a pure Ti coating. For the poisoned mode, at $T < 350$ °C, the matrix will present an oxidation of 7 nm (normally a stainless steel will have a native film of about 3 nm), whereas the oxidation will be of the order of 40 nm for $T > 600$ °C (Fig. 14b).

For coating grown in metallic and transition modes which have a hexagonal TiO_x film at low temperature, there is more oxygen incorporation in the hexagonal structure for the hotter

samples: in metallic mode, Ti at T < 350 °C passes to $TiO_{0.2}$ at T > 600 °C; in transition mode, $TiO_{0.2}$ passes to $TiO_{0.5}$ (information obtained by GIXRD).

For the transition mode, the rutile titanium dioxide thickness passes from 70 nm at T < 350 °C to 150 nm at T > 600 °C. This is due to the presence of both oxygen and high temperature. Rutile is the stable phase of titanium dioxide (see Anatase-Rutile Transformation diagrams), and it was already formed at T < 350 °C, hence it is logical to find it at this temperature.

For the poisoned mode and at T > 600 °C, the chemical composition of the thin film is complex. From Raman spectroscopy, depending on the location, hematite, chromia, and rutile are found. Thanks to a punctual STEM-EDS characterization conducted on a thin lamella (Fig. 14), it appears that the thin film is composed of two main subscales:

- An internal rich Cr oxide.
- And an external Ti oxide which contains some Fe (about 5 to 10 at%).

Consequently, during the PVD poisoned process, the stainless steel is at the same time oxidized while Ti oxide is grown. As already said, at high temperature the stable rutile phase is favored. More importantly, diffusion of the matrix element iron is observed in poisoned mode. Hence, in poisoned mode and at T > 600 °C, the absence of a Ti or TiO_x barrier provokes an oxidation of the matrix and a diffusion of iron into the titanium dioxide phase. To conclude, when the temperature is above 600 °C, there is a modification of the substrate which will have some consequences in the corrosion resistance. It will be the subject of another future paper. High temperature must be generally avoided during the deposition of TiO_x over a stainless steel substrate.

4. Conclusions

Some intermediate conclusion about the characterization may be drawn. *(i)* If the prepared thin lamella is sufficiently thin compared to the grain size of the thin film (thin lamella thickness of 50 nm for grain size of 10 nm), and *(ii)* if ASTAR-TEM is priory associated to

phase identification with XRD, orientation and phase maps can be successfully drawn with a nanometric grain size.

Concerning the process, the stainless steel wire temperature must be controlled in order to avoid metal diffusion (Fe, Ni) from the stainless steel into the TiO_x thin films, and in order not to deteriorate functional properties of the stainless steel as its corrosion resistance.

Rutile or anatase phase may be controlled thanks to the chemical nature of the seed. In this case, only rutile is grown over titanium interlayer whereas both anatase and rutile grains are grown on stainless steel.

By controlling the oxygen partial pressure, the chemical nature of the TiO_x thin films can be tuned from hexagonal titanium with an *x* oxygen content varying from 0.2 to 0.5 until titanium dioxide.

To conclude, the heterogeneous magnetic field and the presence of the anodes cause heterogeneities in the poisoning of the cathode. This evolution in poisoning of the target that covers partially or totally the surface of the cathode results in a chemistry and a microstructure depending on the partial pressure of oxygen: the multilayers pass from titanium to titanium- titanium dioxide, and to titanium dioxide, in metallic, transition, and poisoned modes, respectively. Architectural titanium/ titanium dioxide coating can be directly obtained on stainless steel wire from one wire pass inside the PVD process in an inverted cylindrical magnetron thanks to the continuous mode associated to this plasma heterogeneity. For coloring the wire, the transition zone is of interest for the application searched, even if it comes from a poisoning heterogeneity in the ICM chamber. In fact, it is the only one at which at a pace of 2 mm/s attractive colors such as blue, pink, and green can be obtained with a titanium interlayer.

5. Acknowledgements

This work was performed within the framework of the Centre of Excellence of Multifunctional Architectured Materials 'CEMAM' n°AN-10-LABX-44-01 funded by the "Investments for the Future" Program and supported by Ugitech.

References

[1] P. Roquiny, F. Bodart, G. Terwagne, Colour control of titanium nitride coatings produced by reactive magnetron sputtering at temperature less than 100°C, Surf. Coatings Technol. 116–119 (1999) 278–283. https://doi.org/10.1016/S0257-8972(99)00076-6.

[2] S. Niyomsoan, W. Grant, D.L. Olson, B. Mishra, Variation of color in titanium and zirconium nitride decorative thin films, Thin Solid Films. 415 (2002) 187–194. https://doi.org/10.1016/S0040-6090(02)00530-8.

[3] R. Constantin, J. Matthey, S. Ramseyer, P.-A. Steinmann, Nouveaux revêtements PVD décoratifs résistants à l'usure, Matériaux Tech. 94 (2006) 11–21. https://doi.org/10.1051/mattech.

[4] J.M. Chappé, F. Vaz, L. Cunha, C. Moura, M.C. Marco de Lucas, L. Imhoff, S. Bourgeois, J.F. Pierson, Development of dark Ti(C,O,N) coatings prepared by reactive sputtering, Surf. Coatings Technol. 203 (2008) 804–807. https://doi.org/10.1016/j.surfcoat.2008.05.039.

[5] C. Petitjean, M. Grafouté, C. Rousselot, J.F. Pierson, O. Banakh, A. Cavaleiro, Caractérisation de films colorés de Fe-O-N élaborés par pulvérisation magnétron réactive, Matériaux Tech. 94 (2006) 23–29. https://doi.org/10.1051/mattech.

[6] L. Ćurković, H.O. Ćurković, S. Salopek, M.M. Renjo, S. Šegota, Enhancement of corrosion protection of AISI 304 stainless steel by nanostructured sol-gel TiO2 films, Corros. Sci. 77 (2013) 176–184. https://doi.org/10.1016/j.corsci.2013.07.045.

[7] J.-W. Nah, B.-J. Kim, D.-K. Lee, J.-J. Lee, Color, structure, and properties of TiN coatings prepared by plasma enhanced chemical vapor deposition, J. Vac. Sci. Technol. A Vacuum, Surfaces, Film. 17 (1999) 463–469. https://doi.org/10.1116/1.581607.

[8] S. Konstantinidis, J.P. Dauchot, M. Hecq, Titanium oxide thin films deposited by high-power impulse magnetron sputtering, Thin Solid Films. 515 (2006) 1182–1186. https://doi.org/10.1016/j.tsf.2006.07.089.

[9] Y. Shen, H. Yu, J. Yao, S. Shao, Z. Fan, H. He, J. Shao, Investigation on properties of TiO2 thin films deposited at different oxygen pressures, Opt. Laser Technol. 40 (2008) 550–554. https://doi.org/10.1016/j.optlastec.2007.09.003.

[10] K. Eufinger, D. Poelman, H. Poelman, R. De Gryse, G.B. Marin, Effect of microstructure and crystallinity on the photocatalytic activity of TiO2 thin films deposited by dc magnetron sputtering, J. Phys. D. Appl. Phys. 40 (2007) 5232–5238. https://doi.org/10.1088/0022-3727/40/17/033.

[11] D. Depla, S. Mahieu, Reactive Sputter Deposition, 2008. https://doi.org/10.1117/12.2080955.

[12] S. Takeda, S. Suzuki, H. Odaka, H. Hosono, Photocatalytic TiO2 thin film deposited onto glass by DC magnetron sputtering, Thin Solid Films. 392 (2001) 338–344. https://doi.org/10.1016/S0040-6090(01)01054-9.

[13] B.R. Weinberger, R.B. Garber, Titanium dioxide photocatalysts produced by reactive magnetron sputtering, Appl. Phys. Lett. 66 (1995) 2409–2411. https://doi.org/10.1063/1.113956.

[14] G. Bräuer, B. Szyszka, M. Vergöhl, R. Bandorf, Magnetron sputtering - Milestones of 30 years, Vacuum. 84 (2010) 1354–1359. https://doi.org/10.1016/j.vacuum.2009.12.014.

[15] Gencoa, Speedflo, (n.d.). https://www.gencoa.com/speedflo (accessed December 10, 2019).

[16] C. Nouvellon, M. Michiels, J.P. Dauchot, C. Archambeau, F. Laffineur, E. Silberberg, S. Delvaux, R. Cloots, S. Konstantinidis, R. Snyders, Deposition of titanium oxide films by reactive High Power Impulse Magnetron Sputtering (HiPIMS): Influence of the peak current value on the transition from metallic to poisoned regimes, Surf. Coatings Technol. 206 (2012) 3542–3549. https://doi.org/10.1016/j.surfcoat.2012.02.034.

[17] P. Kofstad, P.B. Anderson, O.J. Krudtaa, Oxidation of titanium in the temperature range 800-1200°C, J. Less-Common Met. 3 (1961) 89–97. https://doi.org/10.1016/0022-5088(61)90001-7.

[18] I. Gurrappa, An oxidation model for predicting the life of titanium alloy components in gas turbine engines, J. Alloys Compd. 389 (2005) 190–197. https://doi.org/10.1016/j.jallcom.2004.05.079.

[19] F.C. Gennari, D.M. Pasquevich, Kinetics of the anatase-rutile transformation in TiO2 in the presence of Fe2O3, J. Mater. Sci. (1998) 1571–1578.

[20] P.A. Cormier, A. Balhamri, A.L. Thomann, R. Dussart, N. Semmar, T. Lecas, R. Snyders, S. Konstantinidis, Titanium oxide thin film growth by magnetron sputtering: Total energy flux and its relationship with the phase constitution, Surf. Coatings Technol. 254 (2014) 291–297. https://doi.org/10.1016/j.surfcoat.2014.06.037.

[21] D. Glöß, P. Frach, O. Zywitzki, T. Modes, S. Klinkenberg, C. Gottfried, Photocatalytic titanium dioxide thin films prepared by reactive pulse magnetron sputtering at low temperature, Surf. Coatings Technol. 200 (2005) 967–971. https://doi.org/10.1016/j.surfcoat.2005.01.018.

[22] P. Frach, K. Goedicke, C. Gottfried, H. Bartzsch, A versatile coating tool for reactive in-line sputtering in different pulse modes, Surf. Coatings Technol. 142–144 (2001) 628–634. https://doi.org/10.1016/S0257-8972(01)01152-5.

[23] E.F. Rauch, M. Véron, Automated crystal orientation and phase mapping in TEM, Mater. Charact. 98 (2014) 1–9. https://doi.org/10.1016/j.matchar.2014.08.010.

[24] L. Latrasse, A. Lacoste, J. Sirou, J. Pelletier, High density distributed microwave plasma sources in a matrix configuration: Concept, design and performance, Plasma Sources Sci. Technol. 16 (2007) 7–12. https://doi.org/10.1088/0963-0252/16/1/002.

[25] A. Todoran, M. Mantel, A. Bés, C. Vachey, A. Lacoste, Control of particle flux and energy on substrate in an inverted cylindrical magnetron for plasma PVD, Plasma Sources Sci. Technol. 23 (2014). https://doi.org/10.1088/0963-0252/23/6/065039.

[26] S. Grosso, L. Latu-Romain, G. Berthomé, G. Renou, T. Le Coz, M. Mantel, Titanium and titanium nitride thin films grown by dc reactive magnetron sputtering Physical Vapor Deposition in a continuous mode on stainless steel wires: Chemical, morphological and structural investigations, Surf. Coatings Technol. 324 (2017) 318–327. https://doi.org/10.1016/j.surfcoat.2017.05.089.

[27] R. Snyders, J.P. Dauchot, M. Hecq, Synthesis of metal oxide thin films by reactive magnetron sputtering in Ar/O2 mixtures: An experimental study of the chemical mechanisms, Plasma Process. Polym. 4 (2007) 113–126. https://doi.org/10.1002/ppap.200600103.

[28] D. Depla, Magnetrons, reactive gases, and sputtering, Diederik Depla, 2017.

[29] J.M. Oh, B.G. Lee, S.W. Cho, S.W. Lee, G.S. Choi, J.W. Lim, Oxygen effects on the mechanical properties and lattice strain of Ti and Ti-6Al-4V, Met. Mater. Int. 17 (2011) 733–736. https://doi.org/10.1007/s12540-011-1006-2.

[30] C. Suryanarayana, M.G. Norton, X-Rays Diffraction: A Practical Approach, Springer, 1998.

[31] D. Rafieian, W. Ogieglo, T. Savenije, R.G.H. Lammertink, Controlled formation of anatase and rutile TiO<inf>2</inf> thin films by reactive magnetron sputtering, AIP Adv. 5 (2015). https://doi.org/10.1063/1.4931925.

[32] P. Löbl, M. Huppertz, D. Mergel, Nucleation and growth in TiO2 films prepared by sputtering and evaporation, Thin Solid Films. 251 (1994) 72–79. https://doi.org/10.1016/0040-6090(94)90843-5.

[33] D.S.R. Krishna, Y. Sun, Z. Chen, Magnetron sputtered TiO2 films on a stainless steel substrate: Selective rutile phase formation and its tribological and anti-corrosion performance, Thin Solid Films. 519 (2011) 4860–4864. https://doi.org/10.1016/j.tsf.2011.01.042.

[34] H. Limage, F.D. Tichelaar, R. Closset, S. Delvaux, R. Cloots, S. Lucas, Study of the effect of a silver nanoparticle seeding layer on the crystallisation temperature, photoinduced hydrophylic and catalytic properties of TiO2 thin films deposited on glass by magnetron sputtering, Surf. Coatings Technol. 205 (2011) 3774–3778. https://doi.org/10.1016/j.surfcoat.2011.01.022.

[35] K.S. Lee, S.H. Lee, Influence of SiO2 interlayer on the hydrophilicity of TiO2/SiO2/glass produced by RF-magnetron sputtering, Mater. Lett. 61 (2007) 3516–3518. https://doi.org/10.1016/j.matlet.2006.11.109.

[36] A.G. Roy, D.E. Laughlin, T.J. Klemmer, K. Howard, S. Khizroev, D. Litvinov, Seed-layer effect on the microstructure and magnetic properties of Co/Pd multilayers, J. Appl. Phys. 89 (2001) 7531–7533. https://doi.org/10.1063/1.1360685.

Tables

Table I Principal element composition of the 316L stainless steel substrate.

Element	Fe	Cr	Ni	Mo	Mn	Si	C
Composition (wt%)	Balance	17	8	2	1.5	0.8	0.03

Table II Growth parameters of the present study.

Deposition mode	Metallic	Transition	Poisoned
ϕ_{O_2}(sccm)	0.5	1.7	3
I_k (A)	2.75	3	2.75
V_k (-V)	302	313	339
p(Ar) (Pa)	0.67	0.67	0.67
ϕ_{Ar} (sccm)	16.5	16.5	16.5
V_A	On	On	On
V_k (-V) for 0 sccm of the day	292	293	274

List of figure captions

Fig. 1 Coated stainless steel reels that were produced in the continuous PVD prototype line described in the present paper.

Fig. 2 Schematic view of the ICM chamber for TiO_x coatings PVD production.

Fig. 3 Diffractograms recorded at low incidence (1.2°) of pure Ti over 316L and of the three modes over 316L: metallic, transition, and poisoned.

Fig. 4 SEM cross-section prepared by FIB (observed in secondary electrons In-Lens detector) of a pure Ti coating grown at 0 sccm of oxygen flux at 2 mm/s. (Growing parameters: I_k = 2.75 A; V_k = 276 V; p(Ar) = 0.67 Pa; ϕ_{Ar} = 16.5 sccm; ϕ_{O_2} = 0 sccm).

Fig. 5 Top: sputtering mode in different zones of the cathode; the center of the cathode is poisoned and the extremities are metallic surfaces. Bottom: deposition rate of Ti grown in static mode as a function of the physical length in the chamber. Zero is the center of the cathode.

Fig. 6 Magnetic field lines in the deposition chamber. The magnetic field is a result of six concentric rings of NdFeB magnets. The 2D simulation of the magnetic field takes into account only the magnets, without taking into account the auxiliary anodes. The permanent magnets are implemented such that their magnetic moments are alternated as follows: N – S – N – S – N –S. The components of the magnetic field are: $B_r = \pm 1{,}47\ T; B_\theta = 0\ T; B_z = 0\ T$.

Fig. 7. A cylindrical titanium cathode (only half of it is presented) after 10 hours of service in the chamber described previously.

Fig. 8 Discharge voltage as a function of the oxygen flow in the chamber. A photography of the wire grown in dynamic conditions, 2 mm/s, to show its color above the corresponding zone.

Fig. 9 MET observations of a TiO_x coating in metallic mode. a) Bright field STEM image and EDS map; the color codes are red for oxygen, yellow for Ti, and green for Fe. b) TEM-ASTAR phase map combined with index map. Good indexations correspond to bright colors. c) TEM-ASTAR orientation map along y direction with corresponding color codes on the right. (Growing parameters: Metallic mode: I_k = 2.75 A; V_k = 302 V; p(Ar) = 0.67 Pa; ϕ_{Ar}= 16.5 sccm; ϕ_{O_2}: 0.5 sccm).

Fig. 10 MET observations of a TiO_x coating in transition mode. a) Bright field STEM image. b) TEM-ASTAR phase map combined with index map. Good indexations correspond to bright colors. The very small blue parts (indexed as rutile) in the hexagonal $TiO_{0.2}$ corresponds to low phase identification reliability and are not significant, this artefact comes from very small grain size in front of the lamella thickness. c) TEM-ASTAR orientation map along y direction with corresponding color codes on the right. (Growing parameters: I_k = 3 A; V_k = 313 V; p(Ar) = 0.67 Pa; ϕ_{Ar}= 16.5 sccm; ϕ_{O_2}: 1.7 sccm).

Fig. 11 TEM observations of a TiO_x coating in poisoned mode. a) Bright field STEM image. b) TEM-ASTAR phase map combined with index map. Good indexations correspond to bright colors. c) TEM-ASTAR orientation map along y direction with corresponding color

codes on the right. (Growing parameters: I_k = 2.75 A; V_k = 339 V; p(Ar) = 0.67 Pa; ϕ_{Ar}= 16.5 sccm; ϕ_{O_2}: 3 sccm).

Fig. 12 TiO_x thin films microstructure description grown continuously as a function of the partial pressure of oxygen.

Fig. 13 Top: Schematic view of the steps to produce the two samples "with and without a Ti interlayer" between the stainless steel substrate and the titanium dioxide coating. Bottom: Raman spectra for two titanium dioxide coatings in poisoned mode. Above: without a titanium interlayer. Below: with a titanium interlayer.

Fig. 14 Bright field STEM image and STEM-EDS map of TiO_x coatings at T > 600 °C. a) Metallic mode (0.5 sccm), zoom of the interface of the coating over the stainless steel matrix; b) poisoned mode (3 sccm).

Figures (without captions, just figure number at the bottom)

Fig. 1

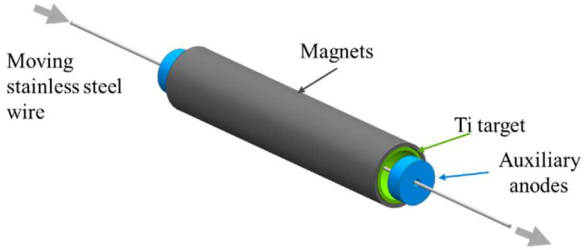

Fig. 2

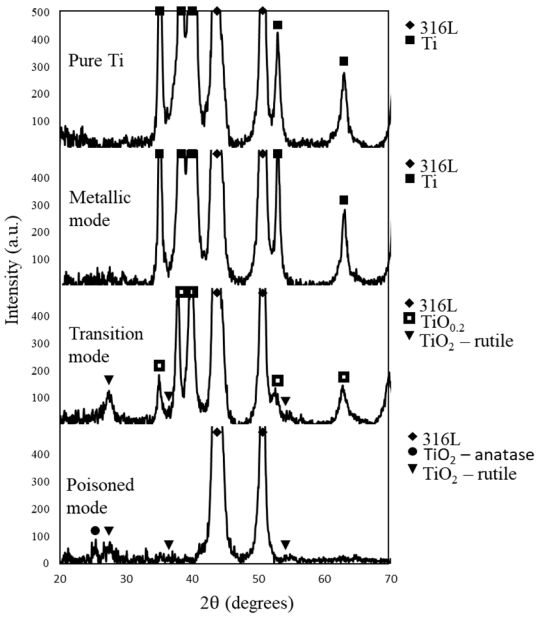

Fig. 3

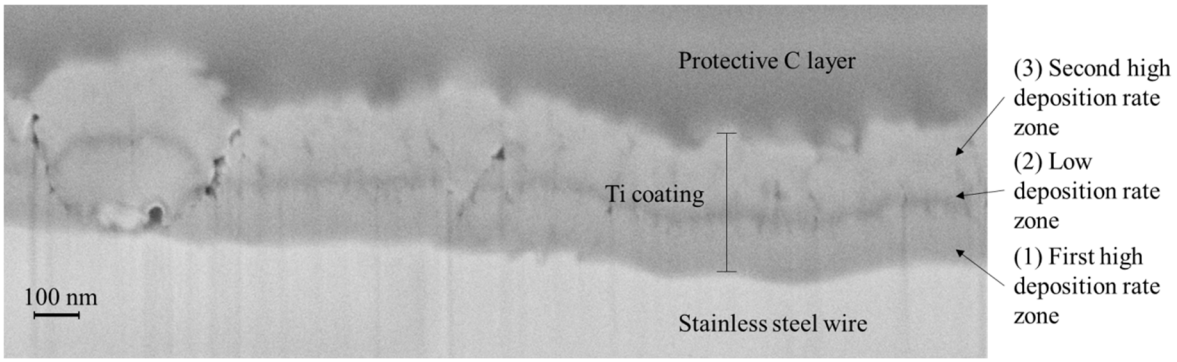

Fig. 4

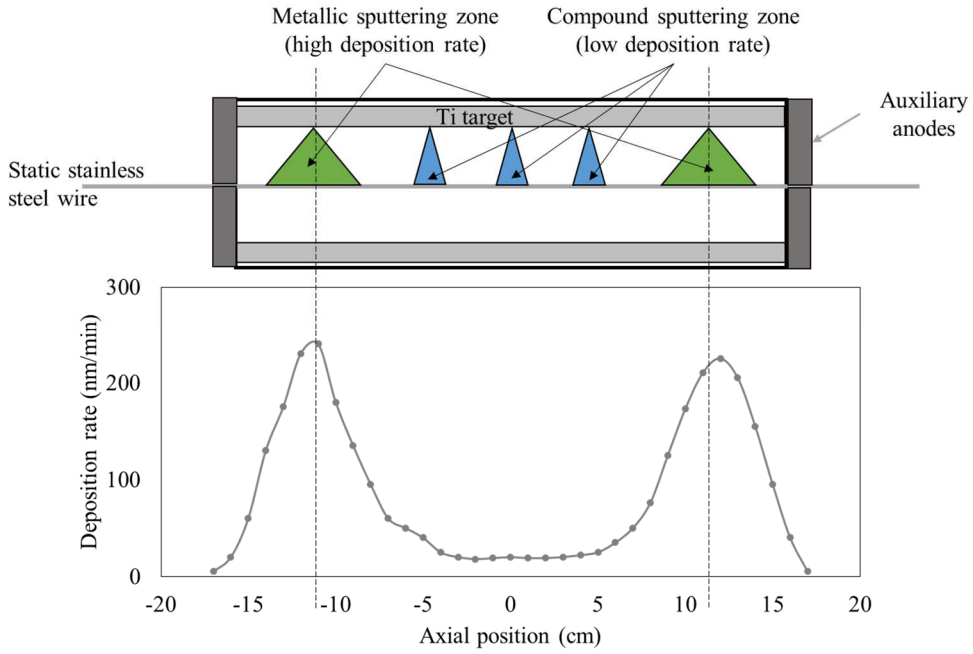

Fig. 5

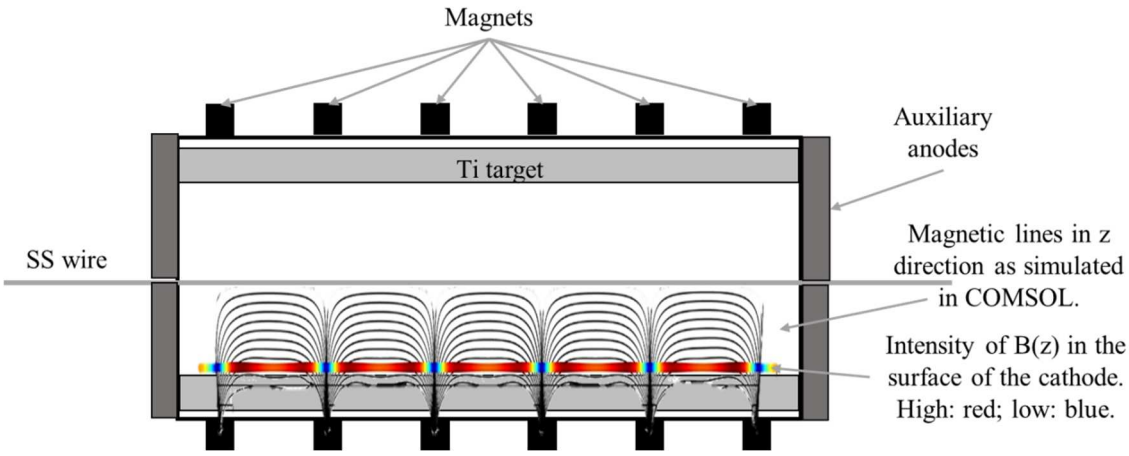

Fig. 6

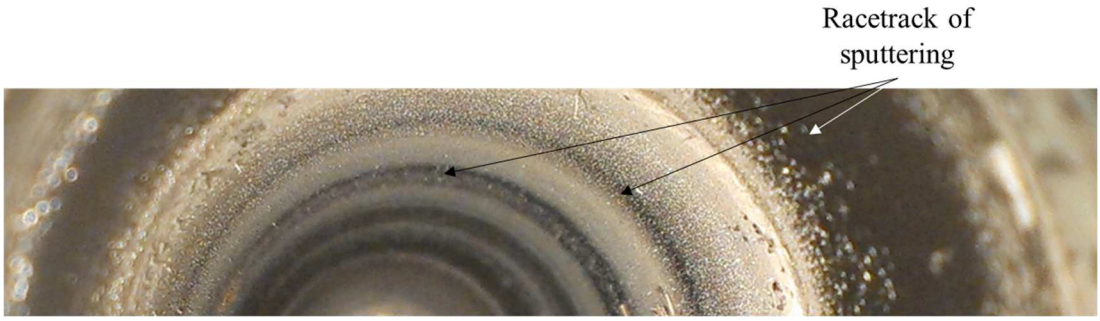
Racetrack of
sputtering

Fig. 7

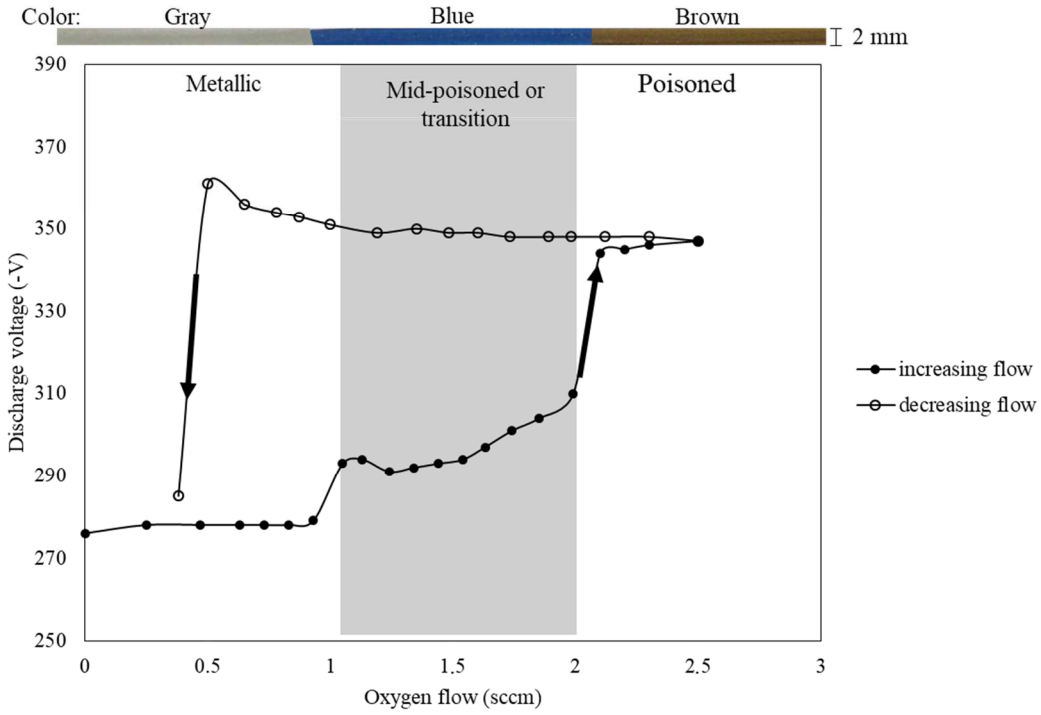
Color:
Gray
Blue
Brown
2 mm
Metallic
Mid-poisoned or
transition
Poisoned
Discharge voltage (-V)
390
370
350
330
310
290
270
250
0
0.5
1
1.5
2
2.5
3
Oxygen flow (sccm)
increasing flow
decreasing flow

Fig. 8

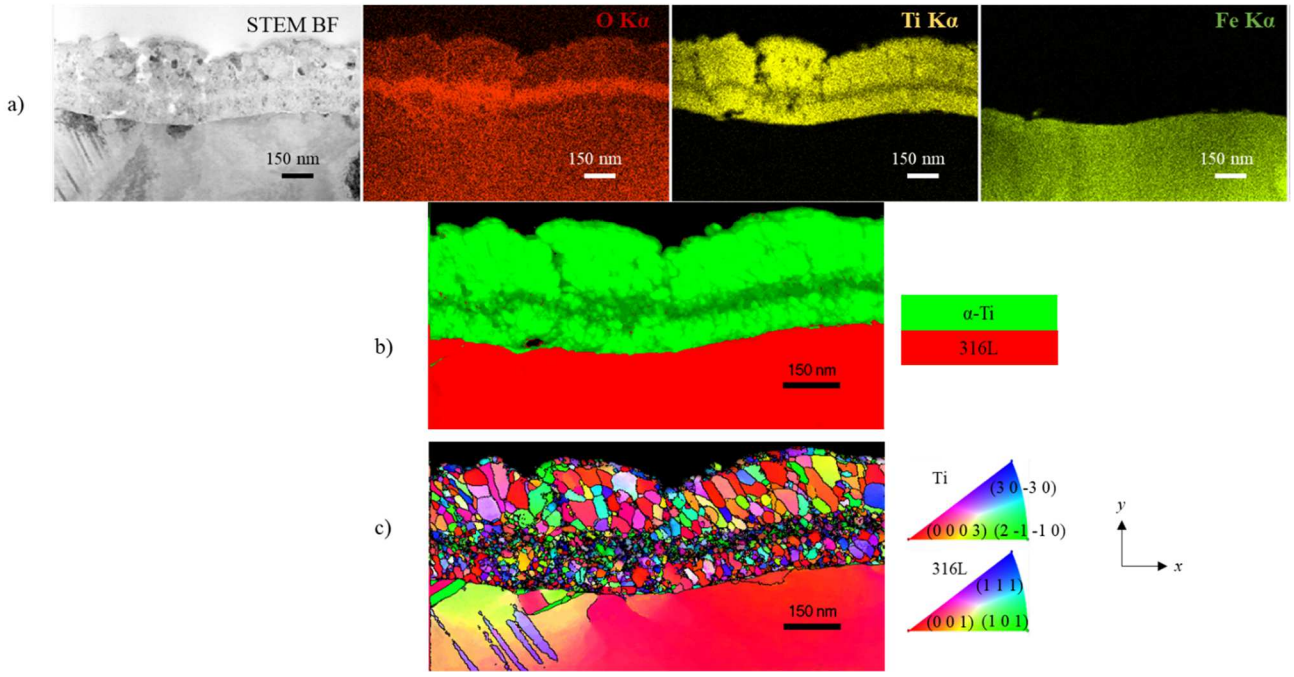
a)
STEM BF
150 nm
O Kα
150 nm
Ti Kα
150 nm
Fe Kα
150 nm
b)
150 nm
α-Ti
316L
c)
150 nm
Ti
(3 0 -3 0)
(0 0 0 3) (2 -1 -1 0)
316L
(1 1 1)
(0 0 1) (1 0 1)
y
x

Fig. 9

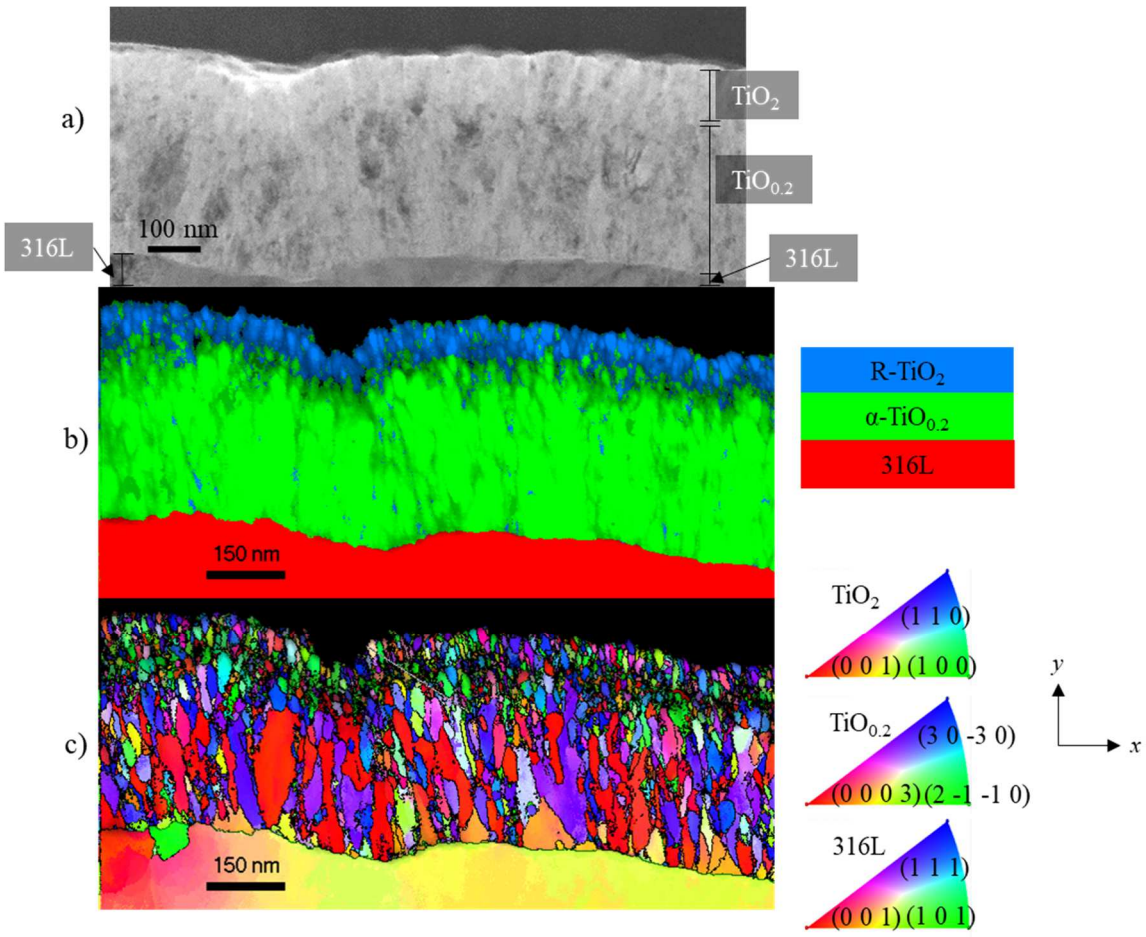
a)
TiO2
TiO0.2
316L
100 nm
316L
b)
150 nm
R-TiO2
α-TiO0.2
316L
c)
150 nm
TiO2
(1 1 0)
(0 0 1) (1 0 0)
TiO0.2
(3 0 -3 0)
(0 0 0 3)(2 -1 -1 0)
316L
(1 1 1)
(0 0 1) (1 0 1)
y
x

Fig. 10

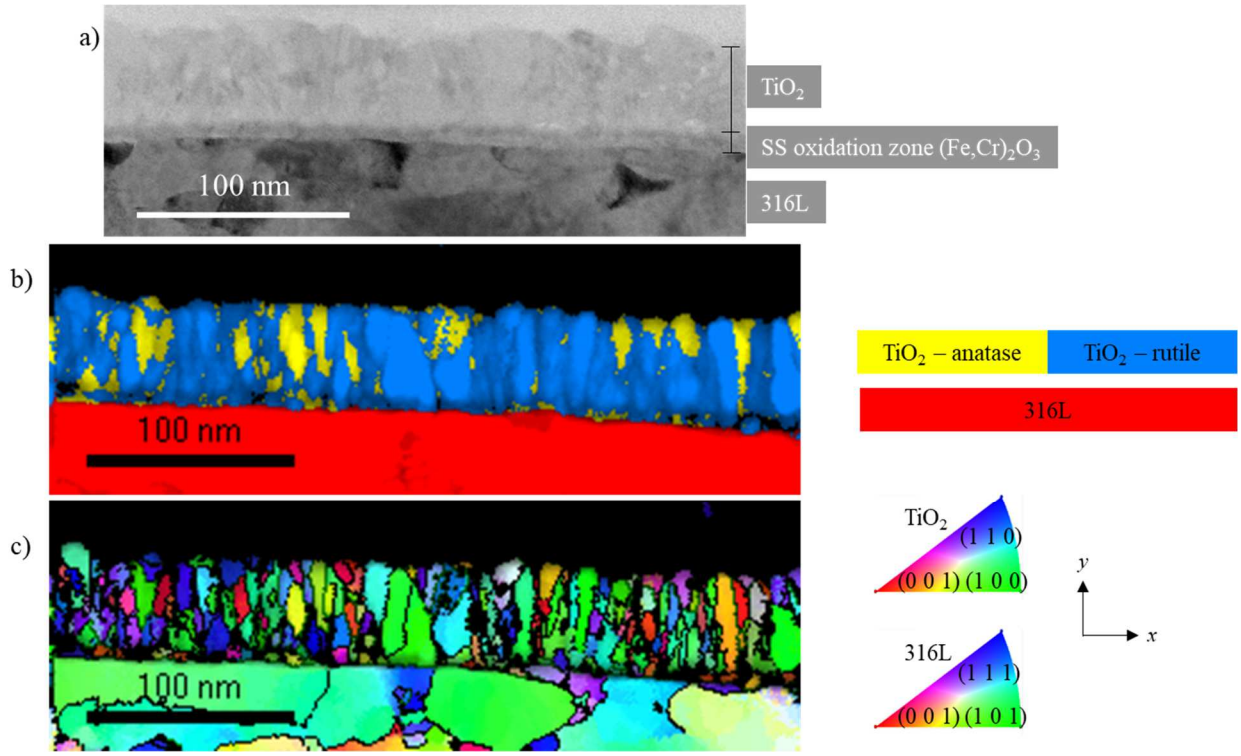
a)
100 nm
TiO2
SS oxidation zone (Fe,Cr)2O3
316L
b)
100 nm
c)
100 nm
TiO2 – anatase
TiO2 – rutile
316L
TiO2
(1 1 0)
(0 0 1) (1 0 0)
316L
(1 1 1)
(0 0 1) (1 0 1)
y
x

Fig. 11

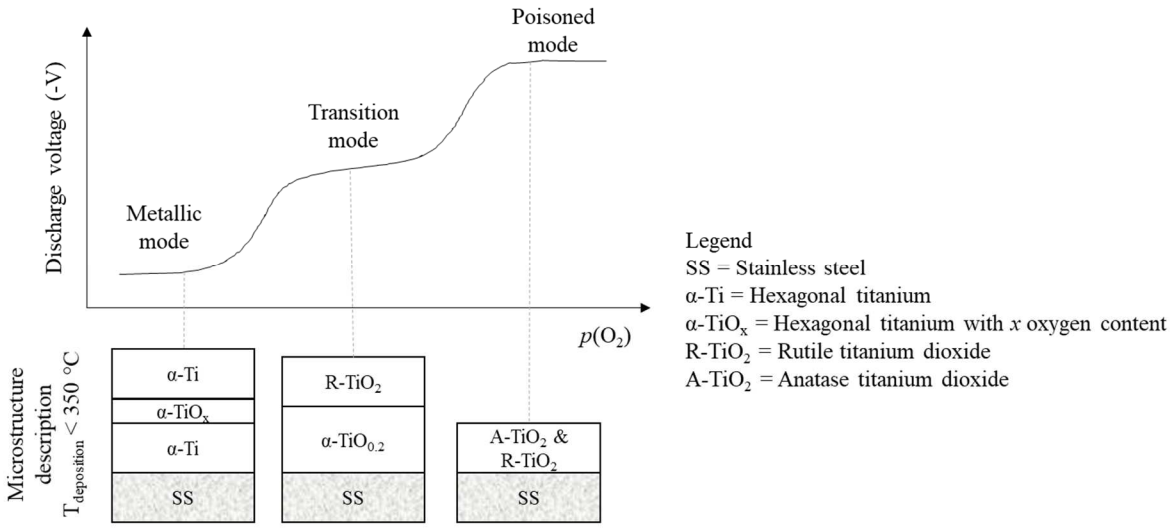
Poisoned mode
Transition mode
Metallic mode
Discharge voltage (-V)
p(O2)
Microstructure description
T deposition < 350 °C
α-Ti
α-TiOx
α-Ti
SS
R-TiO2
α-TiO0.2
SS
A-TiO2 & R-TiO2
SS
Legend
SS = Stainless steel
α-Ti = Hexagonal titanium
α-TiOx = Hexagonal titanium with x oxygen content
R-TiO2 = Rutile titanium dioxide
A-TiO2 = Anatase titanium dioxide

Fig. 12

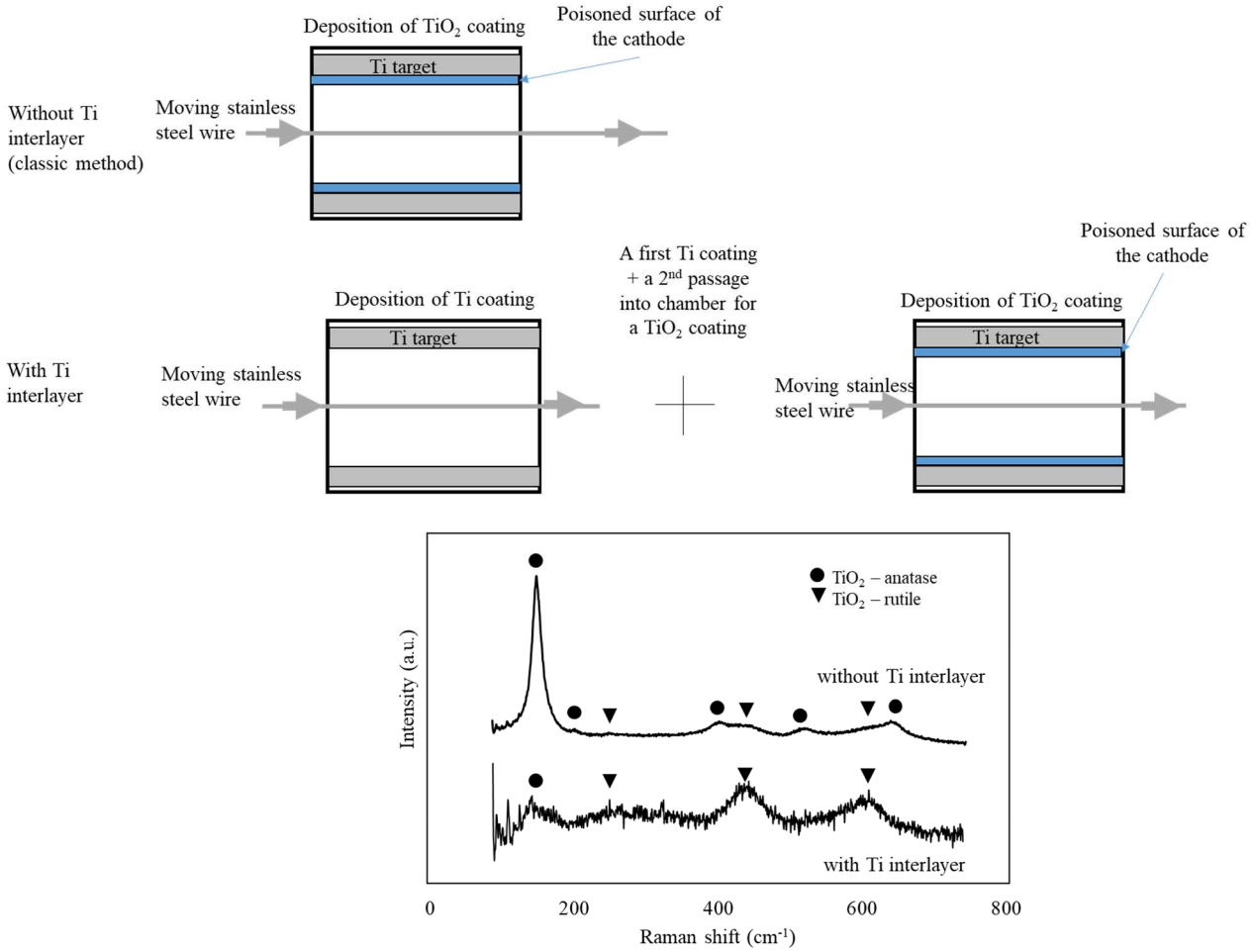
Deposition of TiO_2 coating
Poisoned surface of the cathode
Ti target
Without Ti interlayer (classic method)
Moving stainless steel wire
A first Ti coating + a 2nd passage into chamber for a TiO_2 coating
Deposition of Ti coating
Poisoned surface of the cathode
Deposition of TiO_2 coating
With Ti interlayer
Moving stainless steel wire
Moving stainless steel wire
TiO_2 – anatase
TiO_2 – rutile
without Ti interlayer
with Ti interlayer
Intensity (a.u.)
0
200
400
600
800
Raman shift (cm^{-1})

Fig. 13

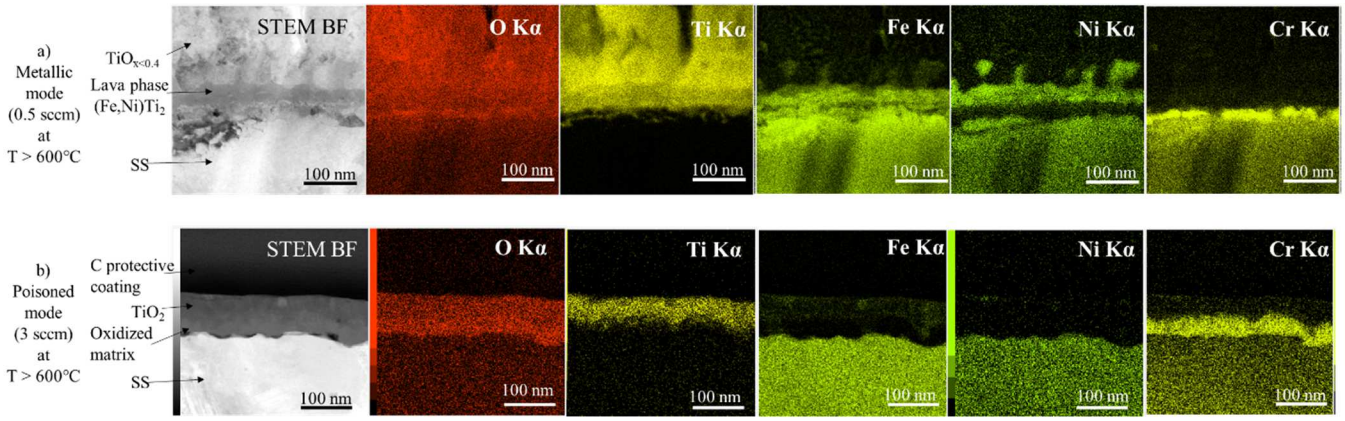
a)
Metallic mode (0.5 sccm) at T > 600°C
$TiO_{x<0.4}$
Lava phase $(Fe,Ni)Ti_2$
SS
STEM BF
O Kα
Ti Kα
Fe Kα
Ni Kα
Cr Kα
100 nm
b)
Poisoned mode (3 sccm) at T > 600°C
C protective coating
TiO_2
Oxidized matrix
SS

Fig. 14